PERGAMON

Radiation Measurements 30 (1999) 609–615

Radiation Measurements

www.elsevier.com/locate/radmeas

An alternative drift shell parameter for modeling trapped particles

Shing F. Fung*, Lun C. Tan

Space Physics Data Facility, Code 632, NASA Goddard Space Flight Center, Greenbelt, MD 20771, USA

Received 5 June 1998; accepted 28 June 1999

Abstract

The McIlwain L parameter has been widely used to label magnetic drift shells of trapped particles. In a dipolar magnetic field, L gives the equatorial radius of a drift shell. When the total magnetospheric magnetic field is significantly altered by the presence of external magnetospheric currents, particularly during geomagnetically active periods, L has to be calculated by using an appropriate magnetic field model that includes the external fields. Thus, an L value computed at a given local time does not always give the position of a drift shell in configuration (real) space, especially at high L values (>4). Since L is one of the magnetic coordinates typically used to organize trapped particle data, the external current effects on the L calculation need to be assessed. In this paper, we show that by conserving the second adiabatic invariant, I, in a model magnetospheric magnetic field given by the sum of the IGRF and the Tsyganenko T89c models, a configuration-space-based drift shell parameter can be defined. It has been found that for a given mirroring field strength B_m on a magnetic field line, the quantity I is empirically related to the radial distance r_t to the point of minimum field strength along that field line. By conserving I, r_t measured in units of Earth radii (R_E) at any local time can be mapped to its equivalent value L_{tn} at noon, and vice versa. We show that L_{tn} can be used as a parameter to label drift shell in configuration space, analogous to the use of L in magnetic space. Published by Elsevier Science Ltd.

1. Introduction

In trapped radiation modeling, the three adiabatic invariants provide the 'natural' coordinates to represent the distribution function of trapped particles (Roederer, 1970; 1996, Schulz, 1996). Conservation of adiabatic invariants of charged particles trapped in the inner magnetosphere also allowed McIlwain (1961) to introduce the L-parameter based on a dipole magnetic field configuration. It has been noted that L can be used to perfectly organize trapped particle directional fluxes perpendicular to the magnetic field, $J_\perp$ (McIlwain, 1966). Particles executing azimuthal drift motions while conserving their invariants will be confined to what is commonly known as a drift shell.

Takahashi et al. (1997), for example, recently examined the radial boundaries of substorm ion injections by attempting to follow the particle drift shells. In the inner radiation belt zone ($1.2 < L \leqslant 3$) where the geomagnetic field can be approximated by a dipole field, the McIlwain L-parameter serves adequately as a drift-shell label and provides a measure of the drift shell radius. In the outer radiation belt zone and beyond ($L > 3$), however, effects of the solar wind and external magnetospheric currents on the geomagnetic field can be significant. Because of the resulting azimuthal asymmetry of the magnetospheric magnetic field, par-

* Corresponding author. Tel.: +1-301-286-6301; fax: +1-301-286-1771.

E-mail address: fung@nssdca.gsfc.nasa.gov (S.F. Fung)

1350-4487/99/$ - see front matter Published by Elsevier Science Ltd.
PII: S1350-4487(99)00243-7

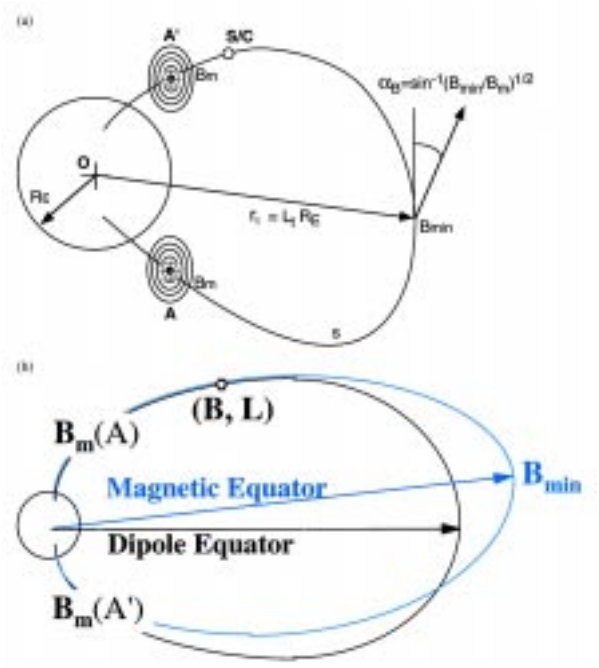

Fig. 1. (a) Schematic view of procedures to determine r_t with α_B being the particle pitch-angle at the $B_{\min}$ point. (b) Mapping of a realistic (distorted) geomagnetic field into a dipole magnetic field.

ticles bouncing along a common field line will follow different azimuthal drift paths, dependent generally upon their equatorial pitch angles and hence B_m. This is the so-called 'shell-splitting' effect (Roederer, 1970) which is best visualized in configuration (real) space. Since a drift shell is identified by specifying both L and B_m, we use the term 'shell-splitting' only to refer to the phenomenon that is commonly known, but not to imply actual splitting of a shell. While it is desirable to have good organization of trapped particle observations in magnetic coordinates, it is also important to visualize the spatial structure of drift shells in real space in order to interpret multi-satellite observations over a wide spatial range.

In order to analyze the behavior of energetic electron fluxes at low altitudes (<1000 km), a suitable parameter is needed to organize the observed particle fluxes into drift shell structure. The McIlwain L-parameter is a perfect parameter for a dipole-field case (McIlwain, 1961). In a realistic field geometry, L actually varies along a field line (McIlwain, 1966) and can no longer be used to visualize drift shell structure in real space. We present in this paper the development of a configuration space-based parameter which can effectively be used to identify drift shells. A requirement of this parameter is that it has to reduce to the L-parameter in the dipole-field limit.

2. Magnetic drift shell and L-parameter

In the limit of a static geomagnetic field, conservation of the first and second adiabatic invariants defines two invariant coordinates for trapped particle motion (Northrop and Teller, 1960): the mirroring field strength,

$$B_m = B/\sin^2\alpha \tag{1}$$

with B and α as the local magnetic field and pitch-angle, and the integral invariant I

$$I = \int_A^{A'} \left[1 - B(s)/B_m\right]^{1/2} \mathrm{d}s \tag{2}$$

with the integration being performed along the field line s between two conjugate mirror points A and A' (Fig. 1(a)). The McIlwain L is then defined as

$$L^3 B_m/M_d = F\left(I^3 B_m/M_d\right) \tag{3}$$

where F is a function which effectively maps any non-dipolar magnetic field into an equivalent dipole field and M_d is the Earth's intrinsic magnetic dipole moment (McIlwain, 1961). It is apparent that when B_m and I are conserved along a particle trajectory, L is also conserved and will thus define a drift shell as the set of field line segments with constant equatorial radial distance $L_0 \equiv (M_d/B_{\min})^{1/3}$ in a dipole field, with $B_{\min}$ being the minimum magnetic field strength of the field line. Eqs. (1) and (2) imply then that (B,L) naturally form a set of equivalent dipole coordinates (see Fig. 1(b)) for locally mirroring particles ($\alpha = 90°$). This coordinate system has been used extensively in trapped radiation modeling (e.g. Sawyer and Vette, 1976; Vette, 1991a,b).

Since B decreases drastically with increasing radial distances, Eq. (2) indicates that for a realistic geomagnetic field configuration I should be a monotonic function of the field line length, which extends with increasing equatorial radial distance r_t to the $B_{\min}$ point. Therefore, for a given $B_m I$ should also be a monotonic function of r_t. However, this relation does not imply that the same r_t at different local times should be associated with the same I value as it does in the dipole field case. As we will show below instead, the inherent asymmetry of a realistic geomagnetic field only allows the use of the same functional form to relate I and r_t at any local time (see Eq. 2); but the parameters in the function can vary with local times.

A realistic geomagnetic field is often distorted by the actions of the solar wind and external magnetospheric currents. Eqs. (2) and (3) for this case indicate that L would actually vary along a field line (McIlwain, 1966). While Eq. (3) provides a definition of L, it does not conveniently give the position of a drift shell in

space (see e.g. Reeves et al., 1991). In order to determine and follow the positions of a drift shell in local time, one has to first trace a magnetic field line and calculate the I value for a given B_m along that field line (Eq. (2)) and compute the corresponding L value (Eq. (3)). The same calculations must be repeated for all model field lines at different local times and radial distances for the same geomagnetic field configuration. Finally, one has to link the real-space positions of those field line segments having the same L value (conserving I and B_m). Without this last step, L cannot be used to identify a drift shell in space. Since the function F is based on a dipole field, which has no inherent local-time asymmetry (Roederer and Schulz, 1969), extreme caution is required in comparing and interpreting trapped radiation data and models results in the B_m-L space, particularly when different magnetic models may have been used in processing the data or constructing the models.

We note also that J. Roederer has defined an L^*-parameter ($L^* = 2\pi M_d/R_E\phi$, with ϕ and R_E being the third adiabatic invariant and Earth's radius, respectively (e.g. see Roederer, 1970)). Like L, L^* does not reflect any azimuthal asymmetry in a magnetic field or distinguish different drift shells enclosing the same ϕ. Such uncertainty becomes more important when effects of various geomagnetic activity levels or magnetospheric states (Fung, 1996) are to be incorporated into the external magnetic field model. Neither L nor L^* can distinguish between different magnetospheric states, although such information may have been implicitly incorporated in the invariant calculations. Therefore, it may be desirable to define a drift-shell parameter that is based on a real-space position in a realistic geomagnetic field, such that a drift shell can be easily identified in real space relative to other magnetospheric boundaries.

3. Magnetic equatorial drift-shell radius, r_t or L_{tn}

Unlike equatorially trapped particles, low-altitude mirroring particles encounter large mirroring fields ($B_m > 1000$ nT) and are less affected by 'shell splitting'. Their drift shells are fairly well defined by their I values, which are effectively given by the length s of the field line along which they bounce (see Eq. (2)). At a given magnetic local time (MLT), s is scaled by its magnetic equatorial radius r_t and the field line is uniquely identified by (r_t, MLT) (Roederer and Schulz, 1969). Due to the inherent asymmetry of a realistic geomagnetic field, r_t is expected to vary with MLT along a given drift shell. As a trapped particle drifts azimuthally around the Earth, it bounces along successive field lines with varying r_t, which reduces to $L(=L_0)$ in the dipole-field limit. Since L_0 is the equatorial radius of a field line in the case of a dipole magnetic field, we will investigate if r_t can effectively serve as a drift shell label in a realistic geomagnetic configuration. We denote the special case of local noon such that $r_t(\mathrm{MLT} = 12\ \mathrm{h}) \equiv L_{tn}$, which we will use as a drift shell label.

Analogous to the McIlwain L and L_π introduced by Roederer and Schulz (1969), L_{tn} is then the radial distance (in R_E) to the magnetic minimum along a given field line in the local noon sector. Unlike L_0, r_t at different local times are not co-planar or limited in the dipole equator plane. Given a realistic magnetic field model, r_t and L_{tn} can be easily computed by simply tracing the field lines and locating the $B_{\min}$ point of each field line. As we shall see below, there is no fundamental difference between L_{tn} and the conventional McIlwain L-parameter to identify a drift shell because they are derived from the same principle, conservation of adiabatic invariants of charged particles in a quasi-static magnetic field. The difference is in their utility in specific applications. While (L_{tn},B_m) and (L,B_m) both specify a drift shell, the parameter L_{tn} explicitly specifies the equatorial radial extent of a drift shell at noon for any realistic magnetic field model; but L does so only for a dipole magnetic field.

4. Empirical relationship between I and r_t

It is clear from Eq. (2) that for a given B_m and MLT, I should scale with r_t. The scaling factors should vary with MLT and geomagnetic configuration (e.g. K_p), reflecting the asymmetry of the total field. Thus for a fixed geomagnetic configuration, a drift shell is simply defined by the locus of r_t along which B_m and I are constant. All the r_t at different MLT can then be mapped (by following the variations of the scaling coefficients with MLT) to its corresponding noon-value L_{tn}. The I-vs-r_t relationship can be modeled empirically at each MLT fairly generally by a second-order polynomial with B_m as a parameter. Thus, for each of the n MLT sectors other than the noon sector, we have

$$I_k = c_{1k}(B_m) + c_{2k}(B_m) r_t + c_{3k}(B_m) r_t^2 \qquad (k = 2, 3, 4, \ldots, n) \tag{4}$$

where $c_{ik}(B_m)$ is the matrix of fitting coefficients. Similarly, at local noon ($k = 1$) we have

$$I_1 = c_{11}(B_m) + c_{21}(B_m) L_{tn} + c_{31}(B_m) L_{tn}^2. \tag{5}$$

By equating $I_k(k = 2\text{-}n)$ in Eq. (4) to I_1 in Eq. (5) for a given B_m and L_{tn}, we can ensure the conservation of B_m and I along a drift shell and solve for r_t at different MLT.

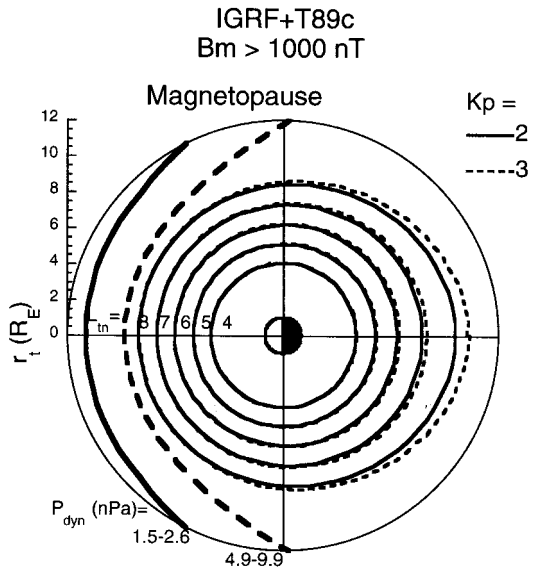

Fig. 2. Loci of r_t for different drift shells as a function of MLT projected onto the GSM X–Y plane under different solar wind dynamic pressure and K_p conditions. Each drift shell is uniquely labeled by its associated L_{tn} value. The magnetopause profiles are as given by Sibeck et al. (1991).

In the present study, the IGRF (1985) internal field and the T89c (Tsyganenko, 1989) external field have been used to model the realistic geomagnetic field. Using this composite field model, we have traced all the model field lines at different MLT (defined by the longitude intercepting the magnetic equator of the field line) and determined all the corresponding r_t to the points of minimum field strength $B_{\min}$. For a range of B_m values, we have calculated all I values associated with the field lines and obtained the real-space contours of each (B_m,I) bin. Fig. 2, taken from Fung and Tan (1998), shows the projections of the loci of r_t as a function of MLT for different drift shells under different solar wind dynamic pressure and K_p conditions. Each drift shell is clearly identifiable by L_{tn}.

5. Mapping between L_{tn} and r_t for low-altitude observations

For any given geomagnetic field configuration, the local-time mapping between L_{tn}, and r_t can be expressed conveniently in terms of the ratio (L_{tn}/r_t) as a function of local time. For low-altitude trapped particles with large $B_m(>10^3$ nT), the $(L_{tn}/r_t)_k$ ratios can be denoted as $(L_{tn}/r_t)_{\infty k}$ because the mapping between L_{tn} and r_t is relatively insensitive to the variation of B_m. For $B_m < 10^3$ nT, $(L_{tn}/r_t)_k$ will depend on B_m because of the 'shell-splitting' effect. It is possible to

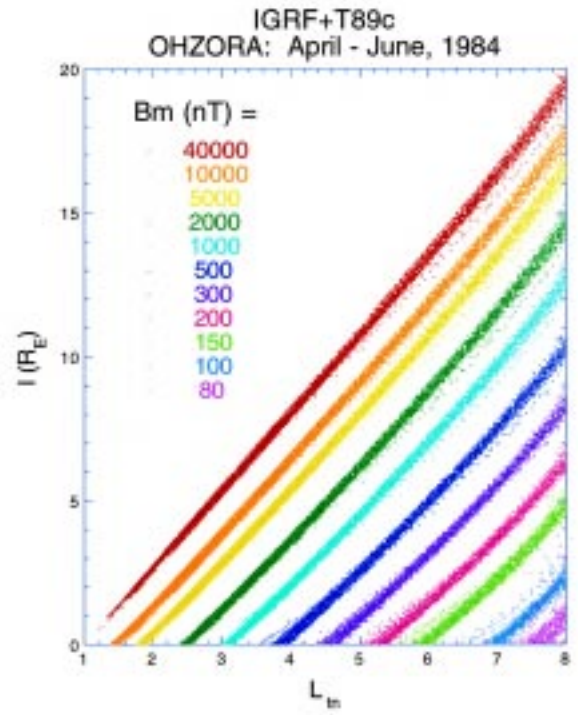

Fig. 3. For various B_m values, I calculated by using the composite IGRF + T89c model are plotted against L_{tn} for all OHZORA positions during April–June, 1984.

combine both the strongly and weakly B_m-dependent cases to obtain an empirical model of the local-time mapping as

$$(L_{tn}/r_t)_k = (L_{tn}/r_t)_{\infty k} + \left[(L_{tn}/r_t)_{0k} - (L_{tn}/r_t)_{\infty k}\right] \exp\left(-\frac{(B_m - B_{m0})}{B_{mck}}\right) \quad (6)$$

where $(L_{tn}/r_t)_{0k}$ is $(L_{tn}/r_t)_k$ at $B_m = B_{m0} = 100$ nT, and B_{mck} is a configuration-dependent characteristic field strength which is determined from $(L_{tn}/r_t)_k$ values calculated for different B_m.

We note that both $(L_{tn}/r_t)_{\infty k}$ and $(L_{tn}/r_t)_{0k}$ can be individually fitted by a second-order polynomial in r_t. Therefore, our mapping can be reduced to a set of coefficient matrices that can be predetermined for any given geomagnetic field configuration. Having these coefficient matrices, a user only needs to perform field tracing to find r_t at an MLT and determine L_{tn} by using Eq. (6) for a given B_m. We have applied this procedure to the real B_m sampled by the Japanese low-altitude (350–850 km) orbiting OHZORA satellite in April–June, 1984 (Nagata et al., 1985). Fig. 3 shows the results of the I-preserving mapping between r_t and L_{tn} for various B_m along all the field lines crossed by

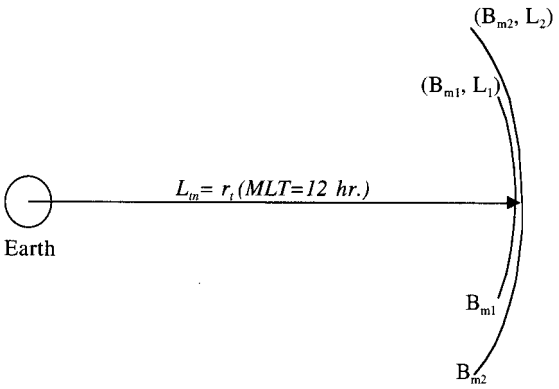

Fig. 4. A schematic illustrating the identification of two drift shells by (B_m,L_{tn}) and (B_m,L) on the same magnetic field line. The parameter L_{tn} generally gives the equatorial radius of the drift shells at noon; whereas L would correspond to the drift shell radii in real space only when the magnetic field is approximated well by a dipole field. The two drift shells (magnetic field line segments) are slightly displaced only for clarity.

the OHZORA satellite. The well-separated color bands for different B_m shown in Fig. 3 indicate that L_{tn} does provide proper ordering of I (c.f. Eqs. (4) and (5)).

Particles with different equatorial pitch angles bounce along different segments (between different sets of mirror points) on the same magnetic field line. An important point to recognize, however, is that all those different segments go through the magnetic equator, at noon and at all other local times, and the location where they do so is organized according to the second invariants (I) of the particles. For trapped particles mirroring at low altitudes along a given field line, their I-values are proportional to the length of the field line, and are thus nearly the same (independent of B_m). On the other hand, particles trapped near the equator at a given local time and radial distance will have different L_{tn} for different B_m. In both situations, L_{tn} gives the equatorial radial extent of a particle drift shell at noon and thus provides an ordering of drift shells, which is more meaningful in configuration space to be referred to as the collection of field lines over which both B_m and I are conserved (see Fig. 3).

A schematic illustrating the identification of drift shells by (B_m,L_{tn}) and (B_m,L) is shown in Fig. 4. It is apparent that for any given spatial location (not necessarily at the magnetic equator) at a reference longitude (e.g. noon), all the drift shells that pass through that location will have the same L_{tn} but only different B_m. On the other hand, different drift shells passing through a given spatial location will have different (B_m,L).

Fig. 5 shows a comparison between L and L_{tn} for two sets of B_m values (>1000 nT and 150 nT) when $K_p=2$. This figure is produced by utilizing the ephe-

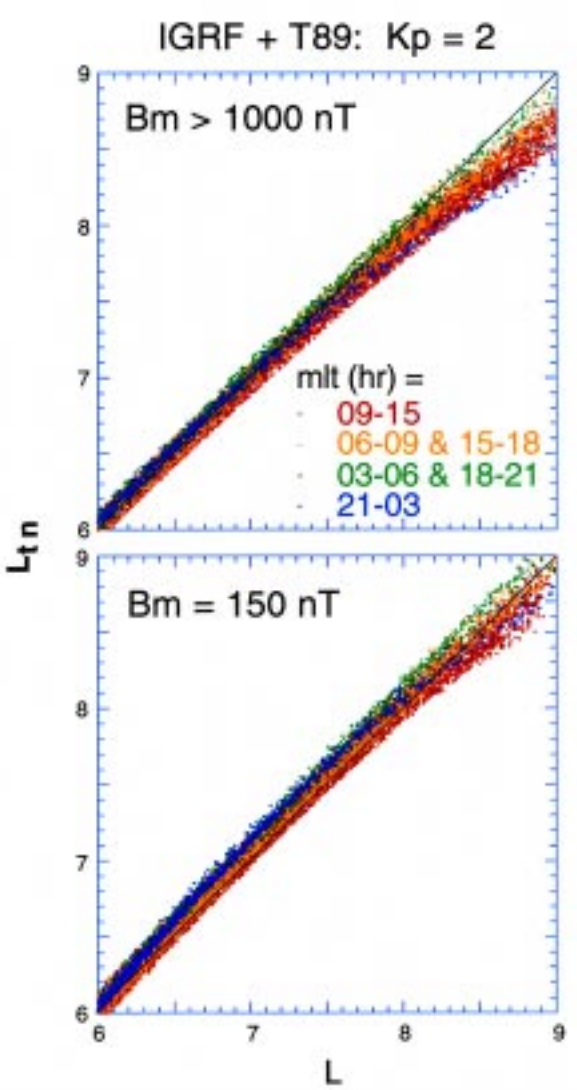

Fig. 5. A comparison between L and L_{tn} for two sets of B_m values (>1000 nT (upper panel) and 150 nT (lower panel)) when $K_p=2$. The solid line $L=L_{tn}$ gives the results expected from a dipole-like internal field only. While there is generally a one-to-one correspondence between L and L_{tn}, external field effects is clearly visible at $L>7$ in the $B_m>1000$ nT case (upper panel).

meris data of the Japanese OHZORA satellite in 1986, which provide a fairly complete sampling of positions over the globe between 350 and 850 km altitudes. For each OHZORA position in a given local time range, the local magnetic field line is traced to calculate r_t and I. Thus for each I value corresponding to each B_m, L and L_{tn} can be computed by using Eqs. (3) and (6), respectively. Since L_{tn} reduces to L in a dipolar field configuration (see Section 3), the solid line $L=L_{tn}$ gives the results expected from only a dipole-like in-

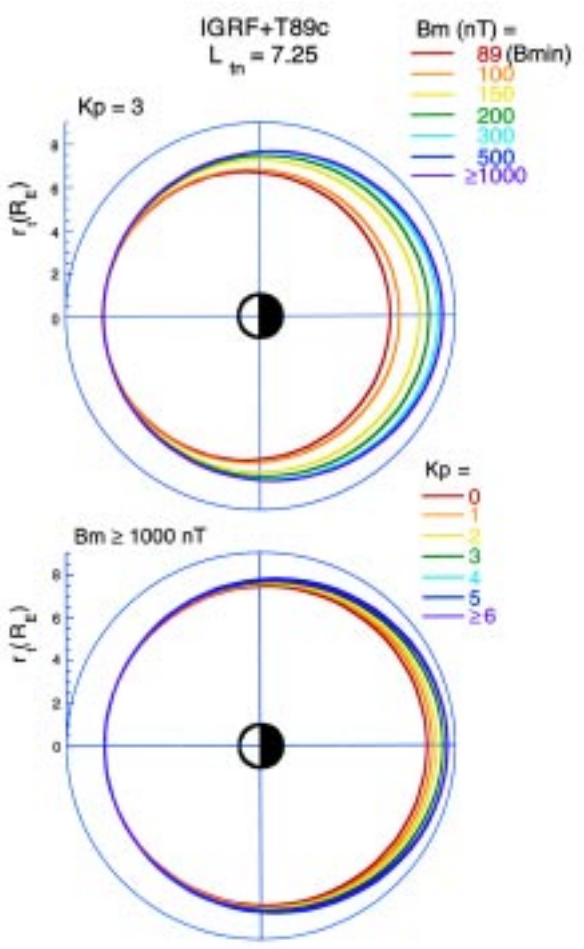

Fig. 6. Plots of r_t as a function of MLT (i.e. different drift shells) at $L_{tn}=7.25$. Here the drift shells for various B_m values at $K_p=3$ (the upper panel), and for different K_p values at $B_m \geqslant 1000$ nT (the lower panel) are shown.

ternal field. It can be seen from Fig. 5 that there is generally a one-to-one correspondence between L and L_{tn}. External field effects is clearly visible at $L > 7$ in the $B_m > 1000$ nT case (upper panel). The scatter in the figure reflects the variations caused by the changing dipole tilt angles, which has not been removed intentionally in order to illustrate its effect.

6. Summary and conclusions

We have developed the use of the radial distances L_{tn} to the magnetic equator at local noon as a new parameter for labeling drift shells of trapped particles. Like the McIlwain L and Roederer L^*, L_{tn} can be used to organize trapped particle observations. Unlike L and L^*, however, L_{tn} can easily be computed and used to identify drift shells in configuration space. Given a geomagnetic field, r_t and MLT can be determined by tracing a field line to its magnetic equator. Then for each MLT sector k, the ordering of I by r_t for various B_m can be empirically modeled by Eqs. (4) and (5). By conserving I in local time for a given B_m, a mapping (Eq. (6)) between r_t at different MLT and L_{tn} at noon then defines a drift shell of all trapped particles with local pitch angle α (see Eq. (1)). Using this mapping, the corresponding L_{tn} value of any arbitrary r_t at any local time can be easily determined.

The direct correspondence of L_{tn} to the equatorial radius of a drift shell at noon allows straightforward visualization of drift shell structure in relation to other magnetospheric boundaries, such as the magnetopause and plasmapause. The I-conserving mapping between L_{tn} and r_t will also show any field asymmetry, whereas the parameter L does not exhibit the asymmetry of a realistic magnetic field. Because L_{tn} is defined in configuration space, drift shell structure will vary with B_m (i.e. 'shell splitting') and geomagnetic activity (e.g. K_p). Fig. 6 (upper panel) shows the 'splitting' of the $L_{tn}=7.25$-shell for different B_m when $K_p=3$. For nearly equatorially trapped particles ($B_m \approx B_{\min}$), r_t at midnight is smaller than that at noon. As B_m increases, however, r_t at midnight gradually increases and eventually exceeds that at noon due to tailward stretching of field lines. 'Shell splitting' is significant only for nearly equatorially trapped particles. Fig. 6 (lower panel) also shows the drift shells of low-altitude trapped particles with $B_m \geqslant 1000$ nT for different K_p. Knowledge of the variations of drift-shell structure with K_p will lead to further understanding of the dynamics of the radiation belts (see e.g. Fung and Tan, 1998).

Acknowledgements

We thank the NASA/National Space Science Data Center (NSSDC) for supplying the IGRF and Tsyganenko models and the OHZORA data. We also thank T. Kohno and K. Nagata for archiving the OHZORA data at the NSSDC. We are also grateful for discussions with C. McIlwain, M. Schulz and D. Boscher. This work was supported by NASA contract NAS 5-97059.

References

Fung, S.F., 1996. Recent development in NASA trapped radiation models. In: Radiation Belts: Models and Standards. AGU, Washington, DC, pp. 79–91 Geophys. Monogr. 97.

Fung, S.F., Tan, L.C., 1998. Time correlation of low-altitude relativistic trapped electron fluxes with solar wind speeds. Geophys. Res. Lett. 25, 2361–2364.

McIlwain, C.E., 1961. Coordinates for mapping the distribution of magnetically trapped particles. J. Geophys. Res. 66, 3681–3691.

McIlwain, C.E., 1966. Comment on the local-time distribution of the geomagnetic field viewed in B–L space. In: McCormac, B.M. (Ed.), Radiation Trapped in the Earth's Magnetic Field. D. Reidel Pub. Co, Dordrect, Holland, pp. 281–283.

Nagata, K., Kohno, T., Murakami, H., Nakamoto, A., Hasebe, N., Takenaka, T., Kikuchi, J., Doke, T., 1985. OHZORA high energy particle observations. J. Geomag. Geoelectr. 37, 329–345.

Northrop, J.G., Teller, E., 1960. Stability of the adiabatic motion of charged particles in the earth's magnetic field. Phys. Rev. 117, 215–225.

Reeves, G.D., Belian, R.D., Fritz, T.A., 1991. Numerical tracing of energetic particle drifts in a model magnetosphere. J. Geophys. Res. 96, 13,997–14,008.

Roederer, J.G., Schulz, M., 1969. Effect of shell splitting on radial diffusion in the magnetosphere. J. Geophys. Res. 74, 4117–4122.

Roederer, J.G., 1970. Dynamics of Geomagnetically Trapped Radiation. Cambridge Univ. Press, New York.

Roederer, J.G., 1996. Introduction to trapped particle flux mapping. In: Radiation Belts: Models and Standards. American Geophys. Union, Washington, D.C, pp. 149–152 Geophys. Monogr. 97.

Sawyer, D.M., Vette, J.I., 1976. AP-8 Trapped Proton Environment for Solar Maximum and Solar Minimum. NASA Goddard Space Flight Center, Greenbelt, Maryland NSSDC/SDC-A-R&S 76-06.

Schulz, M., 1996. Canonical coordinates for radiation-belt modeling. In: Radiation Belts: Models and Standards. American Geophys. Union, Washington, D.C, pp. 153–160 Geophys. Monogr. 97.

Sibeck, D.G., Lopez, R.E., Roelof, R.C., 1991. Solar wind control of the mangetospause shape, location, and motion. J. Geophys. Res. 94, 5489–5495.

Takahashi, K., Anderson, B.J., Ohtani, S-I., Reeves, G.D., Takahashi, S., Sarris, T.E., Mursula, K., 1997. Drift-shell splitting of energetic ions injected at pseudo-substorm onsets. J. Geophys. Res. 102, 22, 117–122, 130.

Tsyganenko, N., 1989. A magnetospheric field model with a warped tail current sheet. Planet. Space Sci. 37, 5–20.

Vette, J.I., 1991a. The NASA/National Space Science Data Center Trapped Radiation Environment Model Program (TREMP) (1964–1991). NASA Goddard Space Flight Center, Greenbelt, Maryland NSSDC/WDC-A-R&S 91-29.

Vette, J.I., 1991b. The AE-8 Trapped Electron Model Environment. NASA Goddard Space Flight Center, Greenbelt, Maryland NSSDC/WDC-A-R&S 91-24.